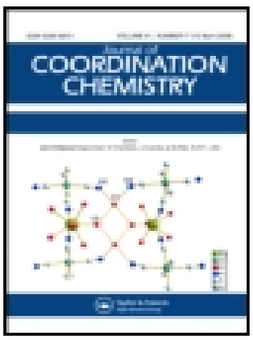

Journal of Coordination Chemistry

ISSN: 0095-8972 (Print) 1029-0389 (Online) Journal homepage: http://www.tandfonline.com/loi/gcoo20

Inhibiting the growth of tumor cells by ruthenium(II) complexes [Ru(phen)$_2$L] (L = o-TFMPIP and p-CPIP) through DNA-binding

Hao Zhang, Li Li, Qiong Wu, Fan Yang, Lanmei Chen, Tieying Hou, Jincan Chen, Wenjie Mei & Xicheng Wang

To cite this article: Hao Zhang, Li Li, Qiong Wu, Fan Yang, Lanmei Chen, Tieying Hou, Jincan Chen, Wenjie Mei & Xicheng Wang (2016): Inhibiting the growth of tumor cells by ruthenium(II) complexes [Ru(phen)$_2$L] (L = o-TFMPIP and p-CPIP) through DNA-binding, Journal of Coordination Chemistry, DOI: 10.1080/00958972.2016.1237633

To link to this article: http://dx.doi.org/10.1080/00958972.2016.1237633

Accepted author version posted online: 16 Sep 2016.
Published online: 16 Sep 2016.

Publisher: Taylor & Francis
Journal: *Journal of Coordination Chemistry*
DOI: http://dx.doi.org/10.1080/00958972.2016.1237633

Inhibiting the growth of tumor cells by ruthenium(II) complexes [Ru(phen)$_2$L] (L = *o*-TFMPIP and *p*-CPIP) through DNA-binding

HAO ZHANG[#a], LI LI[#b], QIONG WU[b], FAN YANG[a], LANMEI CHEN[c], TIEYING HOU[*d,e], JINCAN CHEN[c], WENJIE MEI*[b] and XICHENG WANG*[a]

[a]The First Affiliated Hospital of Guangdong Pharmaceutical University, Guangzhou, 510006, P. R. China
[b]School of Pharmacy, Guangdong Pharmaceutical University, Guangzhou, 510006, P. R. China
[c]College of Pharmacy, Guangdong Medical College, Zhanjiang, Guangdong, 524023, P. R. China
[d]Guangdong Academy of Medical Science, Guangzhou, Guangdong, 510000, P. R. China
[e]Guangdong General Hospital, Guangzhou, Guangdong, 510000, P. R. China

[Ru(phen)$_2$*o*-TFPIP]$^{2+}$ (**1**) and [Ru(phen)$_2$*p*-CPIP]$^{2+}$ (**2**) have been synthesized and demonstrated to inhibit the growth of tumor cells. The inhibitory activities (IC_{50}) of **1** against the growth of C6, MDA-MB-231 and HepG2 cells were about 24.5, 36.7 and 36.1 μM, respectively. Studies show that both complexes bind to CT-DNA, explained by using DFT calculations. The Log*P* calculated for **1** and **2** are -0.4859 and -1.279, respectively. These complexes, especially **1**, can be used as promising inhibitors in chemotherapy, and their DNA binding behaviors play a key role.

Keywords: Ruthenium(II) complex; DNA-binding properties; Antitumor; HOMO; LUMO

1. Introduction

Interactions of transition metal complexes, especially ruthenium(II) complexes, and DNA have been investigated for their potential utility as DNA probes, chemotherapy and photodynamic therapy [1-7]. DNA has long been considered a target for anticancer drugs. Such drugs exhibit DNA-targeted pharmacological activities, impacting DNA replication, an important step in cell growth and cell division, and disturbing transcription and protein synthesis [8, 9]; ruthenium(II) complexes have been reported to bind to DNA by three non-bonding models, intercalating, groove binding and electrostatic binding [10-19].

# These authors contributed equally to the work.

*Corresponding authors. Email: 13902400598@126.com (X. Wang); wenjiemei@126.com (W. Mei); houtieying001@126.com (T. Hou)

Ruthenium(II) complexes are one of the most promising alternatives owing to wide applications as oxidation catalysts, photocatalysts, dye sensitizers for solar cells, DNA probes, protein binding, chemotherapy drugs and photodynamic therapy for tumors. A number of ruthenium(II) complexes have been synthesized. Studies on the interaction of ruthenium(II) complexes indicate that the binding model and affinity of ruthenium(II) complexes depend on the structure of DNA, as well as the structure of metal complexes [16, 20-28]. Ruthenium(II) complexes with large aromatic intercalating ligand and capability for intramolecular hydrogen bonding will bind to DNA with high affinity. Electron withdrawing group in the intercalating ligand improves the DNA-binding affinity of ruthenium(II) complexes [29, 30]. Nevertheless, the interaction of ruthenium(II) complexes with biological macro-molecules is so complicated that new ruthenium(II) complexes with high biological activities are needed.

2. Experimental

2.1. *Chemicals*

Microanalyses were carried out on an Elementar Vario EL elemental analyser. Electrospray experiments were carried out with a Thermo Finnigan LCQ DECA XP ion trap mass spectrometer, equipped with an ESI source. ^{1}H and ^{13}C NMR spectra were recorded on a Varian-300 spectrometer. UV–vis spectra were recorded on a Shimadzu UV-2550 spectrophotometer. The lipo–hydro partition coefficient of these complexes were detected using an octanol–water two-phase system.

2.2. *Synthesis of complexes*

2.2.1. Synthesis of (2-trifloride-phenyl) imidazo[4,5-*f*][1,10]phenanthroline) (*o*-TFPIP).

o-TFPIP was prepared by a similar method to that reported [31], and with some modification. In general, a solution of 1,10-phenanthraquinone (525 mg, 2.5 mmol), ammonium acetate (3.88 g, 50 mmol) and 2-trifluoridphenylaldehyde (609 mg, 3.5 mmol) in 10 ml glacial acetic acid was refluxed for 2 h. The cooled deep red solution was diluted with 25 ml water and neutralized with ammonium hydroxide. Then the mixture was filtered and the precipitates washed with water and acetone, then dried and purified by chromatography over 60-80 mesh SiO_2 using absolute ethanol as eluent. The obtained yield was 516 mg (54%) [32]. Calc. for $C_{20}H_{11}F_3N_4 \cdot H_2O$: C, 62.8; H, 3.43; N, 14.6. Found: C, 61.8; H, 3.64; N, 13.6%. ESI-MS (in CH_3CH_2OH, m/z): 365($[M+H]^+$ cal: 365.09), 387 $[M+Na]^+$, cal: 387.09). ^{1}H NMR (500 MHz, $CDCl_3$) δ 9.04 (dd, J = 4.3, 1.8 Hz, 2H), 8.85 (s, 2H), 7.86 (d, J = 7.8 Hz, 1H), 7.80 (d, J = 7.4 Hz, 1H), 7.75 (s, 1H), 7.73 (t, J = 7.5

Hz, 1H), 7.67 (dd, *J* = 8.1, 4.3 Hz, 3H). ^{13}C NMR (126 MHz, $CDCl_3$) δ 154.82 (s), 154.51 - 154.28 (m), 150.44 (s), 144.70 - 143.48 (m), 138.80 (s), 138.31 (s), 136.57 (d, *J* = 24.5 Hz), 135.66 (d, *J* = 30.9 Hz), 133.05 (s), 131.19 (s), 130.77 (s), 129.54 (d, *J* = 13.9 Hz), 129.02 (s).

2.2.2. Synthesis of (4-carboxyl-phenyl) imidazo[4,5-*f*][1,10]phenanthroline) (*p*-CPIP). *p*-CPIP was prepared as above, but with 1,10-phenanthraquinone (525 mg, 2.5 mmol) and 4-carboxylphenylaldehyde (525 mg, 3.5 mmol), yield: 564 mg (63%) [33]. Calc. for $C_{20}H_{12}N_4O_2 \cdot H_2O$: C, 67.0; H, 3.94; N, 15.6. Found: C, 67.8; H, 4.21; N, 15.2%. ESI-MS (in CH_3CH_2OH, m/z): 341.5($[M+H]^+$, cal: 341.1). ^{1}H NMR (500 MHz, DMSO) δ 13.93 (s, 1H), 9.03 (dt, *J* = 7.2, 3.6 Hz, 2H), 8.91 (dd, *J* = 8.1, 1.7 Hz, 2H), 8.38 (d, *J* = 8.4 Hz, 2H), 8.17 (d, *J* = 8.5 Hz, 2H), 7.83 (s, 2H). ^{13}C NMR (126 MHz, DMSO) δ 168.95 (s), 151.42 (s), 150.05 (s), 145.77 (s), 135.72 (s), 133.29 (s), 132.54 - 131.18 (m), 128.37 (d, *J* = 50.9 Hz), 125.35 (s).

2.2.3. Synthesis of ruthenium(II) complex $[Ru(phen)_2$*o*-TFPIP$]^{2+}$ (1). 1 was synthesized by the literature procedure [34] with some modifications. $[Ru(phen)_2Cl_2] \cdot 2H_2O$ (106 mg, 0.20 mmol) and *o*-TFPIP (76 mg, 0.20 mmol) were added to 10 cm^3 ethylene glycol. The mixture was refluxed for 2 h under an argon atmosphere. The cooled reaction mixture was diluted with water (20 cm^3) and filtered to remove solid impurities. The complex was then separated from soluble impurities by precipitation with $NaClO_4$. The precipitated complex was dried, dissolved in a small amount of MeOH, and purified by chromatography over alumina oxide using MeOH-MeCN (10:1, v/v) as an eluent, yield: 157 mg (73%, calculated from $[Ru(bpy)_2Cl_2] \cdot 2H_2O$). Calc. for $C_{45}H_{31}Cl_2F_3N_8O_8Ru \cdot 2H_2O$: C, 50.2; H, 3.28; N, 10.4. Found: C, 49.7; H, 3.34; N, 10.3%. ESI-MS (in CH_3CN, m/z): 401.33($[M-2(ClO_4)]^{2+}$, cal: 401.5), 801.27($[M-2(ClO_4)-H]^+$, cal: 801). ^{1}H NMR (500 MHz, DMSO) δ 8.97 (d, *J* = 7.8 Hz, 2H), 8.80 – 8.75 (m, 4H), 8.40 (s, 4H), 8.16 (dd, *J* = 5.3, 1.2 Hz, 2H), 8.09 (dd, *J* = 5.2, 1.2 Hz, 2H), 8.04 (d, *J* = 7.9 Hz, 2H), 8.01 (d, *J* = 4.3 Hz, 2H), 7.94 (d, *J* = 3.9 Hz, 2H), 7.88 – 7.85 (m, 2H), 7.82 – 7.75 (m, 4H). ^{13}C NMR (126 MHz, DMSO) δ 168.85 (s), 154.76 (d, *J* = 24.6 Hz), 153.48 (s), 152.64 (s), 149.20 (d, *J* =

10.8 Hz), 147.73 (s), 138.84 (s), 135.13 (s), 134.06 (s), 132.47 (s), 132.27 (s), 130.08 (s), 128.60 (s), 128.32 (s).

2.2.4. Synthesis of ruthenium(II) complex $[Ru(phen)_2p\text{-}CPIP]^{2+}$ (2). The ruthenium(II) complex $[Ru(phen)_2p\text{-}CPIP]^{2+}$ was synthesized with similar method as above, replacing *o*-TFPIP by *p*-CPIP, yield: 170 mg (82%). Calc. for $C_{44}H_{28}Cl_2N_8O_{10}Ru{\cdot}2H_2O$: C, 51.0; H, 3.11; N, 10.8. Found: C, 50.8; H, 3.21; N, 10.6%. ESI-MS (in CH_3CN, m/z): 825.27($[M\text{-}2(ClO_4)\text{-}H]^+$, cal: 825). ^1H NMR (500 MHz, DMSO) δ 9.07 (dd, *J* = 8.3, 1.1 Hz, 2H), 8.79 – 8.76 (m, 4H), 8.43 (d, *J* = 8.6 Hz, 2H), 8.39 (d, *J* = 5.4 Hz, 4H), 8.21 (d, *J* = 8.6 Hz, 2H), 8.14 (d, *J* = 5.3 Hz, 2H), 8.08 (dd, *J* = 5.3, 1.2 Hz, 2H), 8.04 (dd, *J* = 5.3, 1.1 Hz, 2H), 7.82 (s, 2H), 7.77 (dd, *J* = 8.2, 5.3 Hz, 4H). ^{13}C NMR (126 MHz, DMSO) δ 154.93 (s), 154.68 (s), 149.22 (d, *J* = 8.5 Hz), 147.47 (s), 138.80 (d, *J* = 7.4 Hz), 134.66 (s), 134.47 (s), 132.46 (s), 132.27 (s), 130.09 (s), 128.85 (s), 128.35 (s).

2.3. *MTT assay*

To study the cell viability of the complexes, standard 3-(4,5-dimethylthiazole)-2,5-diphenyltetrazolium bromide (MTT) assay procedures were carried out. All complexes were dissolved in DMSO with stock solution at 10 μM. Cells were seeded in 96-well tissue culture plates at 5×10^3 cells/well and incubated in an incubator at 37 °C and 5% CO_2 for 24 h. The cells were then incubated with the tested compounds in a concentration range of 4–300 μM, ensuring an equal volume of 200 μL across the wells of the plate. The plates were incubated at 37 °C in a 5% CO_2 incubator for 72 h. After incubation, 20 μL of yellow tetrazolium salt MTT solution (5 mg mL^{-1}) was added across the plate and further incubated for 4 h. After this time, the medium was aspirated and replaced with a 150 μL/well of DMSO to dissolve the formazan salt formed. The color intensity of the formazan solution, which reflects the cell growth condition, was measured using a microplate spectrophotometer at 490 nm.

2.4. *DNA-binding properties*

2.4.1. Electronic absorption measurements. Electronic absorption titrations (Shimadzu UV-2550 spectrophotometer) were performed to investigate the binding ability with fixed

concentration of Ru(II) complexes (20 μM) but with increasing concentration of calf thymus DNA from 0 to 50 μM. Initially, ruthenium-DNA solutions (3 mL) were allowed to incubate for 5 min before absorption spectra were recorded. Subsequently, the blank buffer solution and the mixed complex sample were placed in the reference and sample quartz cuvettes, respectively. Titration processes were performed until there is no change in the spectrum for at least four titrations, which shows that saturation binding has been reached [35].

2.4.2. Fluorescence emission titrations. Fluorescence experiments were conducted by keeping the concentration of Ru(II) complexes fixed at 20 μM, and at the same time gradually increasing the calf thymus DNA concentration from 0 to 150 μM. Samples were excited at 340 nm, and emission was recorded between 500-700 nm. After the solution was mixed for 2 min, the absorption spectra were recorded [36].

2.4.3. Theoretical section. Both octahedral complexes $[Ru(phen)_2TFPIP]^{2+}$ and $[Ru(phen)_2CPIP]^{2+}$ (shown in scheme 1) form from Ru(II) and one intercalated ligand L and two phen. There is no symmetry in these complexes. The full geometry optimization computations were performed for these complexes applying DFT-B3LYP [37-40] and LanL2DZ basis set [41]. The structural models of the studied compounds are shown in scheme 1 and the singlet state was assumed [42]. All computations were performed with the G98 quantum chemistry program-package [43]. In order to depict the detail of the frontier molecular orbital interactions, stereographs of some related frontier MOs of these complexes were drawn with the Molden v3.6 program [44] based on the obtained computational results.

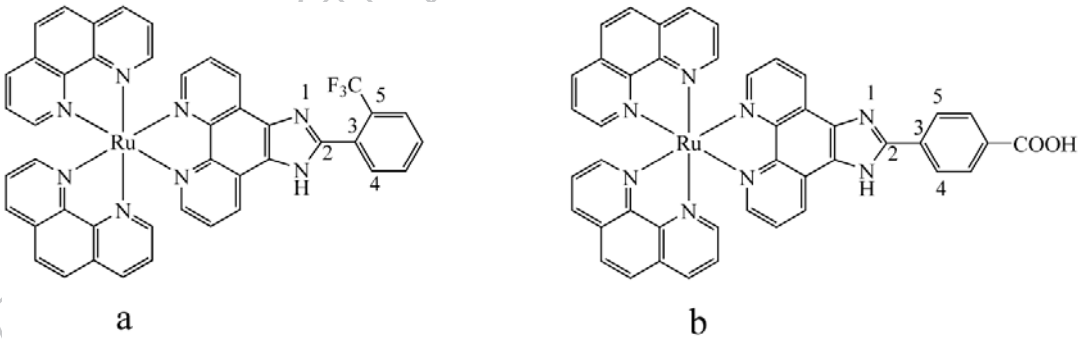

Scheme 1. The molecular structure of ruthenium(II) complexes **1** (a) and **2** (b) [34].

3. Results and discussion

3.1. *Synthesis and characterization*

Ruthenium(II) complexes **1** and **2** were synthesized by refluxing mixture of *cis*-$Ru(phen)_2Cl_2$ and TFPIP or CPIP, respectively. These complexes were obtained as ClO_4^- salts.

In CH_3CN solutions **1** and **2** exhibit a strong IL (intra ligand charge transfer) absorption at 263 and 264 nm, respectively. For **1**, there is a MLCT (metal to ligand charge transfer) absorption from 400 to 700 nm, with maximum at 415 nm, accompanied by a shoulder at 453 nm; for **2**, the MLCT absorption appeared at 458 nm, accompanied by a shoulder at 422 nm.

3.2. *Studies on the antitumor activities*

The inhibitory activity of two Ru(II) complexes against various human tumor cells was evaluated by MTT assay. The complexes exhibited significant inhibition to C6, especially **1**; the inhibitory activity (IC_{50}) of **1** against C6 cells was 24.5 μM, approximately 7.9 times better than that of **2** under the same conditions as shown in table 1. Moreover, the changes in cell viability of the two compounds after 72 h treatment are demonstrated in figure 1. Treatment of rat glioma cell (C6), human breast cancer cell line (MDA-MB-231), human hepatoma G2 (HepG2) and lung adenocarcinoma cell line (A549) cells with **1** and **2** significantly decreased the cell viability in a dose-dependent manner. Compared with **2**, **1** generally has better antitumor activity against different tumor cells. Lipophilicity often plays a role in bioactivity, with proper lipid-water partition coefficients having drugs available for cellular uptake by cells. The Log*P* values calculated for **1** and **2** were -0.486 and -1.279, respectively (table 1). Obviously, **1** is comparatively more lipophilic than **2**, which may result in higher antitumor activity of **1** than **2**. These results suggest that **1** and **2** exhibit inhibition against various tumor cells, especially for sensitive, highly invasive and metastatic cell lines [47, 48].

3.3. *DNA-binding properties*

It is generally accepted that DNA is the target of Ru complexes. To examine whether **1** and **2** can bind to DNA molecules. The interaction between these complexes and DNA was confirmed by spectroscopic analysis.

3.3.1. Electronic spectra. Electronic spectra have been utilized to investigate the DNA binding properties of **1** and **2**. Upon addition of calf-thymus DNA, the MLCT and IL transitions of **1** and

2 undergo hypochromic effect and red shift. The change of electronic spectra of **1** and **2** are shown in figure 2.

In tris-HCl (pH = 7.2) buffer, the MLCT absorption of **1** at 415 nm almost disappeared, and the shoulder moved from 453 to 456 nm. For **2**, the MLCT transition moved from 458 to 453 nm, and the shoulder at 422 nm disappeared. When calf-thymus DNA was added into the ruthenium(II) complex solution, the intensity of both complexes decreased. For **1**, the hypochromic effect is 8% ($\Delta\lambda$=1nm) and for **2**, the hypochromic effect is 9% ($\Delta\lambda$ = 1 nm). These data show that **1** and **2** exhibit great DNA affinity. The intrinsic DNA-binding constants K_b of **1** and **2** can be analyzed with eqn. (1) according to the decay of their MLCT absorption,

$$[DNA]/ \sum_a-\sum_f=[DNA]/\sum_b-\sum_f+1/K_b(\sum_a-\sum_f) \quad (1)$$

where [DNA] is the concentration of DNA in base pairs, $\sum_a$, $\sum_f$ and $\sum_b$, respectively, are equivalent to the extinction coefficient for the free metal complex, complex in the presence of DNA, and complex in fully bound form. In plots of $[DNA]/\sum_a-\sum_f$ versus [DNA], K_b is given by the ratio of slope to intercept. The change of $[DNA]/\sum_a-\sum_f$ following the concentration of [DNA] of **1** and **2** are shown in figure 2c and 2d.

For **1**, the ratio of slope of plot of $[DNA]/\sum_a-\sum_f$ versus [DNA] is different at low DNA concentration and high DNA concentration, indicating there are two different binding processes in the interaction with DNA. The binding constants calculated for low DNA concentration and high DNA concentration are 42.6 and 5.81×10^4, respectively. For **2**, there is only one slope ratio observed for the plots of $[DNA]/\sum_a-\sum_f$ versus [DNA], indicating only one binding mechanism with DNA, and the calculated binding constant is 8.55×10^4. These data also show that **1** binds less tightly to double-strand helix DNA than **2** at high DNA concentration.

3.3.2. Fluorescence emission spectra. Fluorescence emission spectra of **1** and **2** were also studied in the absence and presence of calf-thymus DNA, as shown in figure 3.

At room temperature, when excited at 470 nm, **1** and **2** exhibit strong emission spectra from 500-700 nm excited at 350 nm, with maxima at 589 and 590 nm, respectively. For **1**, when calf-thymus DNA was added to the solution, the emission decreased at first; when the ratio of [DNA]/[Ru] reached 0.1, the emission intensity for both complexes are lowest, and the relative emission strengths (I/I_0) for **1** and **2** are 0.97 and 0.93, respectively. The emission intensity for **1** and **2** increased, and at [DNA]/[Ru] = 2 the relative intensities for **1** and **2** are 1.22 and 1.44, respectively. With addition of CT-DNA, the fluorescence first decreased and then increased as

shown in figure 3. The fluorescence intensity as a function of blend ratio indicates miscibility for both complexes and CT-DNA. It is reasonable to assume that for the CT-DNA any electronic interaction between the ruthenium(II) complex is small except for that at the interfaces because the phase separation occurs macroscopically. At high concentration of DNA, ruthenium(II) complex can effectively bind DNA molecules.

To further clarify the DNA-binding of **1** and **2**, the emission titration was carried out in the presence of calf-thymus DNA. The change of emission spectra for **1** and **2** in increasing DNA concentration is shown in figure 3c.

The emission strength of **1** and **2** decreased at low DNA concentration, while the emission strength increased at higher DNA concentration. At low [DNA] / [Ru] ratio, there is energy transfer between the double-strand helix DNA and ruthenium(II) complexes; when the concentration of DNA increased, the ruthenium(II) complexes were protected by the hydrophobic double-strand helix DNA from quenching by water molecules. These data, together with electronic spectra, show that there may be a two-step binding mechanism in the interaction of these ruthenium(II) complexes and DNA molecules. For **1**, the binding affinity is higher at low DNA concentration than that at high DNA concentration, while for **2**, there is no obvious difference in binding affinity at low DNA concentration and high DNA concentration. Both complexes exhibited DNA-binding ability.

3.3.3. Theoretical computations. We could not obtain the crystal structures of **1** and **2**. Theoretical computations by the DFT method were utilized to understand the structures and DNA interactions; calculated bond lengths, bond angles and dihedral angles of **1** and **2** are listed in table 2. As shown in table 2, the dihedral angles of **1** and **2** are 55.7 and 2.3 degrees (N1-C2-C3-C5) (figure 4a), respectively. These data show that the intercalating ligand of **1** is not planar. So it is predictable that **2** will bind to DNA much stronger than **1**, since the interaction of ruthenium(II) and DNA depends on the planarity of the intercalating ligand.

Based on the computed results, some frontier molecular orbital energies and total energies, the schematic diagram of the energies and related ^{1}MLCT transitions, and the molecular orbital stereographs of $[Ru(phen)_2L]^{2+}$ are given in table 3, figures 4b and 5, respectively.

According to frontier molecular orbital theory [49, 50], for a reaction controlled by orbital interactions between reactant molecules, electrons are more easily transferred from Highest Occupied Molecular Orbital (HOMO) of one reactant to Lowest Unoccupied Molecular Orbital (LUMO) of another; thus reactions are more advantageous between one reactant molecule with higher HOMO energy and another molecule with lower LUMO energy. There are π–π interactions in the DNA binding of these complexes in intercalation mode. Kurita and Kobayashi [49] reported a simple calculation model by the DFT method for stacked DNA base-pairs with backbones, and the computed HOMO and Next-to-Highest Occupied Molecular Orbital (NHOMO) energies of the DNA section model with base pairs are much higher (-1.27 and -1.33 eV) than our computed LUMO and NLUMO (NL) energies (< -7.0 eV) of $[Ru(phen)_2L]^{2+}$ (L = *o*-TFPIP and *p*-CPIP). Such a trend in relative energies will be retained in our ruthenium(II)-DNA macromolecule system because the attraction between electrons in metal oxide semiconductor (MOs) and metal complex cations with high positive charges is much stronger than that of DNA. Thus electrons are transferred more easily from the HOMO of DNA to the LUMO of complex intercalating to DNA helix, and it can be predicated that those complexes bind to DNA more tightly with lower energies of LUMO. The LUMO energies of **1** and **2** are -0.2689 and -0.2700 a.u., respectively. These data show that the energy of the LUMO of **1** is higher than that of **2**, indicating that **1** may bind to DNA less strongly than that of **2**.

Ji *et al*. reported that ruthenium(II) complexes with electron-acceptor group in intercalating ligand bind to DNA more tightly. Considering both **1** and **2** have similar structures, the electron parameters for $–CF_3$ group and –COOH group obtained from reference [48] are 0.43 and 0.45. Again the higher electron-withdrawing –COOH group was predicted to increase the DNA binding affinity of **2**.

4. Conclusion

We have synthesized two new potential antiproliferative agents, $[Ru(phen)_2o\text{-TFPIP}]^{2+}$ (**1**) and $[Ru(phen)_2p\text{-CPIP}]^{2+}$ (**2**), which show high cytotoxicity and excellent DNA activities compared with other ruthenium complexes [28, 51-55]. According to the MTT results, these complexes exhibit antitumor activities against a panel of human cancer cell lines, especially for C6, MDA-MB-231 and HepG2 cells. In addition, interactions with calf-thymus DNA have been investigated by spectroscopic methods. A two-step binding mechanism

occurred in the interaction of **1** with DNA, and the calculated intrinsic DNA binding constant for **1** at low DNA concentration is 4.26×10^5 and 5.81×10^4 at high DNA concentrations. For **2**, there are no detectable differences in the binding affinity between low DNA concentration and high DNA concentration, and the binding affinity is 8.55×10^4. The difference between DNA-binding affinities has been explained by calculation using density functional theory (DFT), and the results show the less tight DNA-binding affinity of **1** can be attributed to the non-planarity of MHPIP and the high energies of LUMO of **1**. These results suggest that these complexes may exhibit effective antineoplasmic activity through binding DNA.

Acknowledgements

The authors acknowledge the National Nature Science Foundation of China (81572926), the Provincial Major Scientific Research Projects in Universities of Guangdong Province (2014KZDXM053), the Science and Technology Project of Guangdong Province (2014A020212312), the Science and Technology Projects of Yuexiu District (2014-WS-039), and the Joint Natural Sciences Fund of the Department of Science and Technology and the First Affiliated Hospital of Guangdong Pharmaceutical University (GYFYLH201309).

References

[1] S.M. Guichard, R. Else, E. Reid, B. Zeitlin, R. Aird, M. Muir, M. Dodds, H. Fiebig, P.J. Sadler, D.I. Jodrell. *Biochem. Pharmacol*., **71**, 408 (2006).

[2] F. Pierard, A. Kirsch-De Mesmaeker. *Inorg. Chem. Commun*., **9**, 111 (2006).

[3] C. Scolaro, T.J. Geldbach, S. Rochat, A. Dorcier, C. Gossens, A. Bergamo, M. Cocchietto, I. Tavernelli, G. Sava, U. Rothlisberger, P.J. Dyson. *Organometallics*, **25**, 756 (2006).

[4] M. Brindell, E. Kulis, S.K. Elmroth, K. Urbanska, G. Stochel. *J. Med. Chem*., **48**, 7298 (2005).

[5] W.J. Mei, J. Liu, K.C. Zheng, L.J. Lin, H. Chao, A.X. Li, F.C. Yun, L.N. Ji. *Dalton Trans*., 1352 (2003).

[6] H. Chao, W.-J. Mei, Q.-W. Huang, L.-N. Ji. *J. Inorg. Biochem*., **92**, 165 (2002).

[7] E. Paleček, M. Bartošík. *Chem. Rev*., **112**, 73 (2012).

[8] G.R. Fulmer, A.J.M. Miller, N.H. Sherden, H.E. Gottlieb, A. Nudelman, B.M. Stoltz, J.E. Bercaw, K.I. Goldberg. *Organometallics*, **29**, 2176 (2010).

[9] X. Wang, Z. Guo. *Chem. Soc. Rev*., **42**, 202 (2013).

[10] Y. Xiong, X.-F. He, X.-H. Zou, J.-Z. Wu, X.-M. Chen, L.-N. Ji, R.-H. Li, J.-Y. Zhou, K.-B. Yu. *J. Chem. Soc., Dalton Trans*., 19 (1999).

[11] L. Ji, Q. Zhang, J. Liu. *Sci. China, Ser. B*, **44**, 246 (2001).

[12] P. Lincoln, B. Nordén. *J. Phys. Chem. B*., **102**, 9583 (1998).

[13] Y. Xiong, L.N. Ji. *Coord. Chem. Rev*., **185**, 711 (1999).

[14] J.G. Liu, B.H. Ye, H. Li, L.N. Ji, R.H. Li, J.Y. Zhou. *J. Inorg. Biochem*., **73**, 117 (1999).

[15] G. Ruchi, M. Lallan. *Inorg. Chem*., **51**, 3059 (2012).

[16] J. Wang, Y. Chen, J. Ren, C. Zhao, X. Qu. *Nucleic Acids Res*., **42**, 3792 (2014).

[17] J.P. Hall, K. O'Sullivan, A. Naseer, J.A. Smith, J.M. Kelly, C.J. Cardin. *Proc. Natl. Acad. Sci*., **108**, 17610 (2011).

[18] H. Niyazi, J.P. Hall, K. O'Sullivan, G. Winter, T. Sorensen, J.M. Kelly, C.J. Cardin. *Nat. Chem*., **4**, 621 (2012).

[19] H. Song, J.T. Kaiser, J.K. Barton. *Nat. Chem*., **4**, 615 (2012).

[20] J.-H. Tan, Y.-J. Lu, Z.-S. Huang, L.-Q. Gu, J.-Y. Wu. *Eur. J. Med. Chem*., **42**, 1169 (2007).

[21] L.-F. Tan, X.-J. Chen, J.-L. Shen, X.-L. Liang. *J. Chem. Sci*., **121**, 397 (2009).

[22] S. Thota, S. Vallala, M. Imran, S. Mekala, S.S. Anchuri, S.S. Karki, R. Yerra, J. Balzarini, E.D. Clercq. *J. Coord. Chem*., **66**, 1031 (2013).

[23] S. Fukuzumi, M. Tanaka, M. Nishimine, K. Ohkubo. *J. Photochem. Photobiol., A*, **175**, 79 (2005).

[24] K.N. Kumar, R. Ramesh, L. Yu. *J. Inorg. Biochem*., **100**, 18 (2006).

[25] E. Ioachim, E.A. Medlycott, G.S. Hanan, F. Loiseau, S. Campagna. *Inorg. Chim. Acta*, **359**, 766 (2006).

[26] S. Thota, S. Vallala, R. Yerra, D.A. Rodrigues, E.J. Barreiro. *Int. J. Biol. Macromol*., **82**, 663 (2016).

[27] J.Q. Wang, P.Y. Zhang, Q. Chen, X.J. Hou, L.N. Ji, C. Hui. *Eur. J. Biochem*., **19**, 335 (2014).

[28] J.-Q. Wang, Z.-Z. Zhao, H.-B. Bo, Q.-Z. Chen. *J. Coord. Chem*., **69**, 177 (2016).

[29] M. Shilpa, C. Shobha Devi, P. Nagababu, J. Naveena Lavanya Latha, R. Pallela, V. Rao Janapala, K. Aravind, S. Satyanarayana. *J. Coord. Chem*., **66**, 1661 (2013).

[30] L. Jie, W.J. Mei, L.J. Lin, K.C. Zheng, C. Hui, F.C. Yun, L.N. Ji. *Inorg. Chim. Acta*, **357**, 285 (2004).

[31] E.A. Steck, A.R. Day. *J. Am. Chem. Soc.*, **65**, 452 (1943).

[32] Y. Du, X. Fu, H. Li, B. Chen, Y. Guo, G. Su, H. Zhang, F. Ning, Y. Lin, W. Mei. *ChemMedChem.*, **9**, 714 (2014).

[33] J. F. Yin, D. Bhattacharya, P. Thanasekaran, C.P. Hsu, T.W. Tseng, K.L. Lu. *Inorg. Chim. Acta*, **362**, 5064 (2009).

[34] R. Hage, J.G. Haasnoot, J. Reedijk, R. Wang, E.M. Ryan, J.G. Vos, A.L. Spek, A.J.M. Duisenberg. *Inorg. Chim. Acta*, **174**, 77 (1990).

[35] Q. Wu, C. Fan, T. Chen, C. Liu, W. Mei, S. Chen, B. Wang, Y. Chen, W. Zheng. *Eur. J. Med. Chem.*, **63**, 57 (2013).

[36] W.J. Mei, Y.X. Liu, J. Liu, J. Li, K.C. Zheng, L.N. Ji. *Transition Met. Chem.*, **30**, 82 (2005).

[37] A.D. Becke. *J. Chem. Phys.*, **98**, 1372 (1993).

[38] J. Foresman, E. Frish. Gaussian Inc., Pittsburgh, USA (1996).

[39] A. Görling. *Phys. Rev. A*, **54**, 3912 (1996).

[40] P. Hohenberg. *Phys. Rev.*, **136**, 864 (1964).

[41] P.J. Hay, W.R. Wadt. *J. Chem. Phys.*, **82**, 299 (1985).

[42] A. Juris, V. Balzani, F. Barigelletti, S. Campagna, P.L. Belser, A. Von Zelewsky. *Coord. Chem. Rev.*, **84**, 85 (1988).

[43] G. Schaftenaar, CMBI, Faculty of Science, University of Nijmegen, The Netherlands (1999).

[44] C. Scolaro, A. Bergamo, L. Brescacin, R. Delfino, M. Cocchietto, G. Laurenczy, T.J. Geldbach, G. Sava, P.J. Dyson. *J. Med. Chem.*, **48**, 4161 (2005).

[45] I. Turel, J. Kljun, F. Perdih, E. Morozova, V. Bakulev, N. Kasyanenko, J.A. Byl, N. Osheroff. *Inorg. Chem.*, **49**, 10750 (2010).

[46] M.S. Burkhead, H. Wang, M. Fallet, E.M. Gross. *Anal. Chim. Acta*, **613**, 152 (2008).

[47] I. Fleming, *Frontier Orbitals and Organic Chemistry Reactions* (1976).

[48] K. Fukui, T. Yonezawa, H. Shingu. *J. Chem. Phys.*, **20**, 722 (1952).

[49] N. Kurita, K. Kobayashi. *Comput. Chem.*, **24**, 351 (2000).

[50] A. Leo, D. Hoekman: *Exploring QSAR*, American Chemical Society (1995).

[51] X.L. Hong, W.G. Lu. *J. Coord. Chem.*, **68**, 4408 (2015).

[52] X.W. Liu, J.S. Shu, X. Yang, Y.M. Shen, S.B. Zhang, J.L. Lu. *J. Coord. Chem.*, **68**, 2886 (2015).

[53] C. Wang, Q. Wu, Y. Zeng, D. Huang, C. Yu, X. Wang, W. Mei. *J. Coord. Chem.*, **68**, 1489 (2015).

[54] Z. Zhang, W. Mei, X. Wu, X. Wang, B. Wang, S. Chen. *J. Coord. Chem.*, **68**, 1465 (2015).

[55] J. Sun, W.X. Chen, X.D. Song, X.H. Zhao, A.Q. Ma, J.X. Chen. *J. Coord. Chem.*, **68**, 308 (2014).

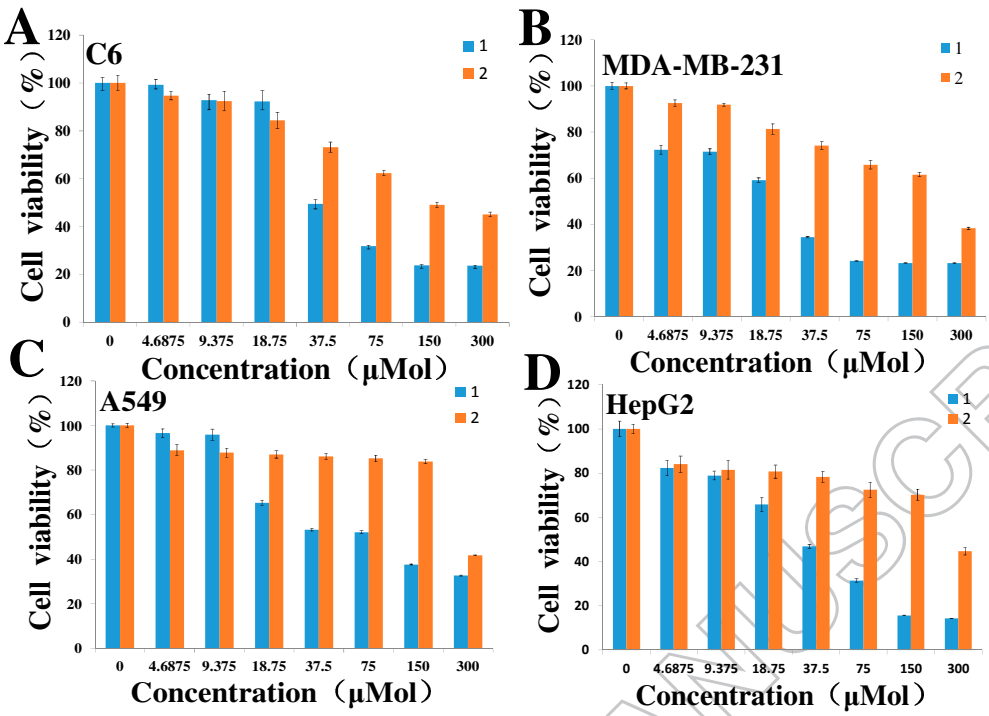

Figure 1. *In vitro* cell viabilities of C6 (A), MDA-MB-231 (B), A549 (C) and HepG2 (D) cells incubated with **1** and **2** at 37 °C for 72 h.

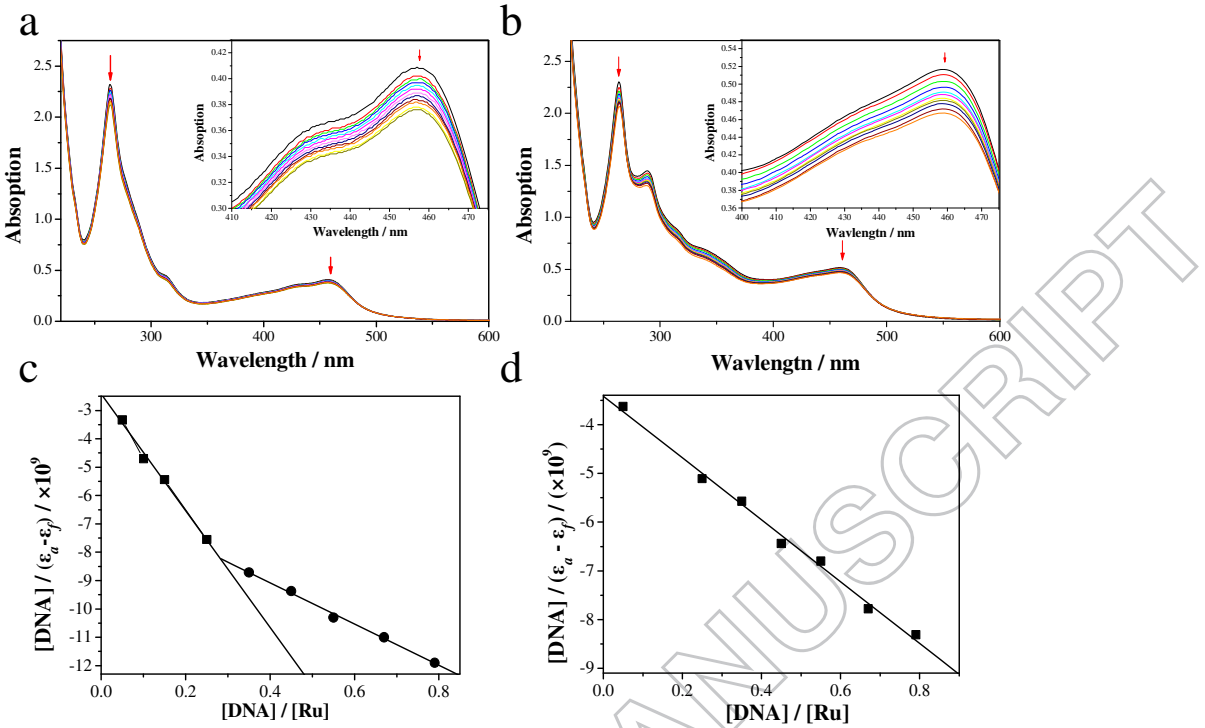

Figure 2. The electronic spectra of **1** (a) and **2** (b) in the absence and presence of calf-thymus DNA. [Ru] = 20 μM. The change of [DNA]/$\sum_a$-$\sum_f$ following the concentration of [DNA] of **1** (c) and **2** (d).

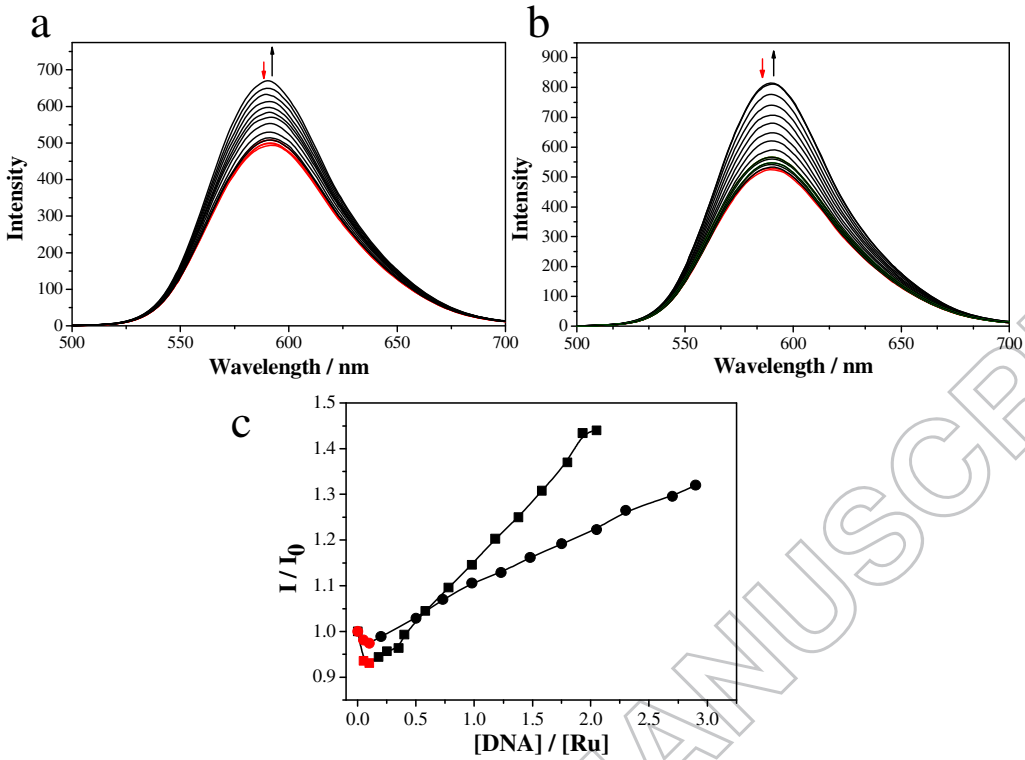

Figure 3. The emission spectra of **1** (a) and **2** (b) in the absence and presence of calf-thymus DNA. [Ru] = 20 μM. The change of emission strength of **1** (•) and **2** (■) in increasing amounts of calf-thymus DNA (c).

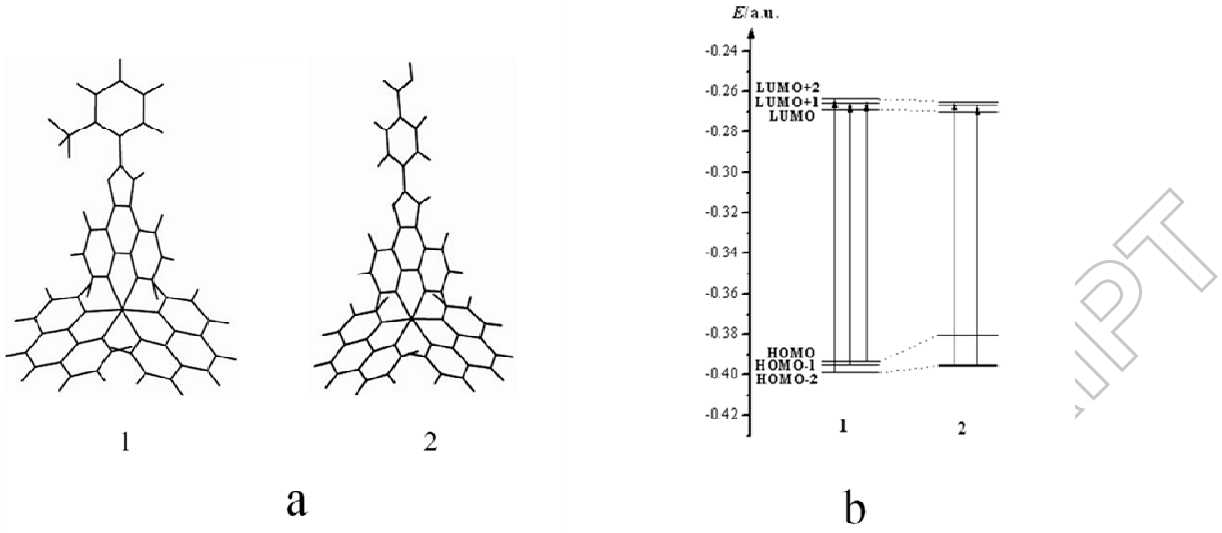

Figure 4. Calculated geometric structures of **1** and **2** (a); schematic diagrams of some frontier MO energies and the related MLCT transitions of **1** and **2** (b).

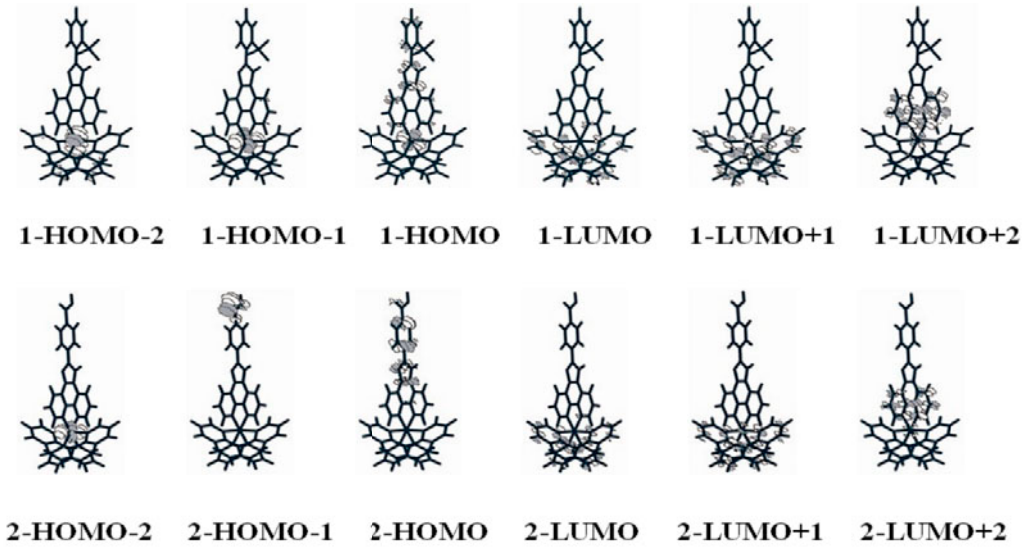

Figure 5. Some related frontier MO stereographs of ruthenium(II) complexes **1** and **2**.

Table 1. The inhibitory activity (IC_{50}/μM) of **1** and **2** against selected cell lines.

Compound	Inhibitory activity/IC_{50}					Log P
	C6	HepG2	MDA-MB-231	A549	MCF-7	
1	24.5±0.6	36.1±0.9	36.7±0.5	84±1	119±1	-0.486
2	195±6	254±10	199±4	255±4	>300	-1.279

Table 2. Bond lengths, bond angles and dihedral angles of **1** and **2**.

Compound	Bond length/nm				Bond angle/°		Dihedral angle/°	
	$Ru–N_m$[a]	$Ru–N_{co}$	$C–C(N)_m$[b]	$C–C(N)_{co}$	A_m[c]	A_{co}	N1-C2-C3-C4	N1-C2-C3-C5
1	0.2103	0.2107	0.1408	0.1406	79.3	79.4	-123.3	55.7
2	0.2105	0.2107	0.1407	0.1406	79.3	79.4	-177.6	2.3

[a]$Ru\text{-}N_m$ expresses the mean coordination bond length between Ru and N of the main ligand and $Ru\text{-}N_{co}$ expresses that between Ru and N of the coligand (phen). [b]$C\text{-}C(N)_m$ expresses the mean bond length of the ring skeleton of the main ligand. [c]A_m expresses the coordination bond angle between Ru and two N of the main ligand.

Table 3. Some frontier molecular orbits energies (εi/a.u.) for **1** and **2**.

Compound	H-3	H-2	H-1	HOMO	LUMO	L+1	L+2	Dc_{L-H}	Dc_{L-NH}
1	-0.4031	-0.3989	-0.3949	-0.3934	-0.2689	-0.2651	-0.2633	0.1245	0.1260
2	-0.3990	-0.3958	-0.3953	-0.3804	-0.2700	-0.2663	-0.2645	0.1104	0.1253

Graphical abstract